AGU PUBLICATIONS

Geochemistry, Geophysics, Geosystems

RESEARCH ARTICLE
10.1002/2014GC005638

Key Points:
- Splay faults intercept and transmit deeply sourced fluids
- The distribution of dehydration fluids is controlled by thermal structure
- Results provide mechanism for the formation of mud volcanoes on the upper slope

Correspondence to:
R. M. Lauer,
rlauer@ucsc.edu

Citation:
Lauer, R. M., and D. M. Saffer (2015), The impact of splay faults on fluid flow, solute transport, and pore pressure distribution in subduction zones: A case study offshore the Nicoya Peninsula, Costa Rica, *Geochem. Geophys. Geosyst.*, *16*, 1089–1104, doi:10.1002/2014GC005638.

Received 28 OCT 2014
Accepted 12 MAR 2015
Accepted article online 20 MAR 2015
Published online 18 APR 2015

The impact of splay faults on fluid flow, solute transport, and pore pressure distribution in subduction zones: A case study offshore the Nicoya Peninsula, Costa Rica

Rachel M. Lauer[1] and Demian M. Saffer[2]

[1]Department of Earth and Planetary Sciences, University of California, Santa Cruz, California, USA, [2]Department of Geosciences and Center for Geomechanics, Geofluids, and Geohazards, Pennsylvania State University, University Park, Pennsylvania, USA

Abstract Observations of seafloor seeps on the continental slope of many subduction zones illustrate that splay faults represent a primary hydraulic connection to the plate boundary at depth, carry deeply sourced fluids to the seafloor, and are in some cases associated with mud volcanoes. However, the role of these structures in forearc hydrogeology remains poorly quantified. We use a 2-D numerical model that simulates coupled fluid flow and solute transport driven by fluid sources from tectonically driven compaction and smectite transformation to investigate the effects of permeable splay faults on solute transport and pore pressure distribution. We focus on the Nicoya margin of Costa Rica as a case study, where previous modeling and field studies constrain flow rates, thermal structure, and margin geology. In our simulations, splay faults accommodate up to 33% of the total dewatering flux, primarily along faults that outcrop within 25 km of the trench. The distribution and fate of dehydration-derived fluids is strongly dependent on thermal structure, which determines the locus of smectite transformation. In simulations of a cold end-member margin, smectite transformation initiates 30 km from the trench, and 64% of the dehydration-derived fluids are intercepted by splay faults and carried to the middle and upper slope, rather than exiting at the trench. For a warm end-member, smectite transformation initiates 7 km from the trench, and the associated fluids are primarily transmitted to the trench via the décollement (50%), and faults intercept only 21% of these fluids. For a wide range of splay fault permeabilities, simulated fluid pressures are near lithostatic where the faults intersect overlying slope sediments, providing a viable mechanism for the formation of mud volcanoes.

1. Introduction

In subduction zones, porous sediments on the incoming plate are subjected to a progressive increase in tectonic and overburden stress as they are accreted to the upper plate or subducted with the downgoing plate. The stress increase is initially borne by the fluid, creating a pressure gradient that drives flow. Dissipation of these pressures leads to rapid consolidation and dewatering [e.g., *Shipley et al.*, 1990; *Bekins and Dreiss*, 1992; *Saffer et al.*, 2000], which is generally most pronounced near the trench, where compressible, high porosity sediments are initially subjected to tectonic loading [e.g., *Bray and Karig*, 1985; *Bekins and Dreiss*, 1992; *Saffer and Tobin*, 2011]. In addition to fluids derived from compaction, subducted sediments host bound water that becomes an important source of fluids at depths $>\sim$3–5 km, where temperatures are sufficient to drive dehydration reactions [e.g., *Moore and Vrolijk*, 1992]. The fluid flow driven by these dewatering processes plays a key role in volatile, heat, and solute transport though the forearc.

Excess pore pressure generated by loading and dehydration reactions also exerts a primary control on the mechanical behavior of faults and sediments by mediating effective stress [e.g., *Byerlee*, 1990; *Moore and Vrolijk*, 1992; *Scholz*, 1998; *Kitajima and Saffer*, 2012]. For example, elevated pore pressure, possibly linked to metamorphic dehydration reactions, is hypothesized to cause transitional slip behavior on faults over a wide range of depths, including episodic tremor [*Peacock*, 2009], low-frequency earthquakes and tremor [*Shelley et al.*, 2006; *Liu and Rice*, 2007; *Kitajima and Saffer*, 2012], and silent-slip or slow slip events [*Kodaira et al.*, 2004; *Bell et al.*, 2010]. The exhaustion of thermally driven smectite dehydration, which constitutes the largest shallow release of bound water in most subduction zones, has been suggested to mark the updip

limit of the seismogenic zone, because the associated increase in effective stress would facilitate stick-slip behavior [e.g., *Scholz*, 1998; *Moore and Saffer*, 2001; *Spinelli and Saffer*, 2004; *Ranero et al*., 2008].

The distribution of excess pore pressure, in combination with the hydraulic architecture of the forearc, defines fluid, heat, and solute flow paths and rates [e.g., *Cutillo et al*., 2003; *Lauer and Saffer*, 2012]. Fluids sampled at seafloor seep sites and in boreholes at convergent margins are commonly geochemically distinct from seawater and characterized by reaction products derived from deeper in the subduction zone [e.g., *Kastner et al*., 1991; *Hensen et al*., 2004; *Sahling et al*., 2008; *Ranero et al*., 2008]. In many cases, these observations document that faults cutting the upper plate play a key role in transporting fluids and solutes from the slab to the seafloor [*Hensen et al*., 2004; *Teichert et al*., 2005; *Ranero et al*., 2008; *Sahling et al*., 2008; *Reyners and Eberhart-Phillips*, 2009]. The primary source of dehydration-derived fluid in the outer forearc is the transformation of smectite to illite clay [*Bethke*, 1986; *Moore and Vrolijk*, 1992; *Kastner et al*., 1993; *Bekins and Dreiss*, 1994], which occurs over a temperature range of ~60–150°C and is strongly controlled by reaction kinetics, and the geologic sedimentary environment [*Freed and Peacor*, 1989, 1992]. The locus of smectite dehydration is intimately tied to the subducted sediment composition, the thermal structure of the subduction zone, and the plate convergence rate, all of which vary between margins and along-strike of individual subduction zones [e.g., *Underwood*, 2002, 2007; *Saffer et al*., 2008].

Previous modeling studies aimed at quantifying pore pressure and fluid flow patterns in subduction zones have generally assumed a simplified permeability structure that includes only the main plate boundary or sand layers as permeable conduits [*Bekins et al*., 1995; *Saffer and Bekins*, 1998; *Henry*, 2000; *Matmon and Bekins*, 2006; *Spinelli et al*., 2006]. Despite the observation that splay faults are common at both accretionary and nonaccretionary subduction zones, and geochemical and hydrological data that suggest they represent important hydraulic connections from the plate interface below, few modeling studies have quantitatively explored their effects [e.g., *Cutillo et al*., 2003; *Shi and Wang*, 1988; *Lauer and Saffer*, 2012].

Here we address this problem using a 2-D numerical model of coupled fluid flow and transport, using the well-studied Nicoya margin of Costa Rica as an example. Specifically, we investigate (1) the role of splay faults in controlling the budgets and patterns of fluid egress and solute transport; (2) the relationship between the thermal structure of the forearc, the locus of clay dehydration reactions, and resulting fluid geochemistry and transport patterns; and (3) the implications for pore pressure translation and the formation of mud volcanoes.

2. Geologic Setting of the Nicoya Margin

2.1. Tectonic and Thermal Setting

The Middle America trench is formed by northeastward subduction of the Cocos plate beneath the Carribean plate at a rate of ~85 mm/yr [*DeMets*, 2001, Figure 1a]. Offshore of the Nicoya Peninsula, the subducted crust is uniform in age (~20–25 Ma), but divided between crust formed at the Cocos-Nazca Spreading Center (CNS) to the southeast, and crust formed at the East Pacific Rise (EPR) to the northwest [*Barkhausen et al*., 2001]. The Nicoya region experiences large megathrust earthquakes ($Mw > 7$) approximately every 50 years [e.g., *Protti et al*., 2014]. The seismogenic zone, defined on the basis of local and regional earthquake studies [*DeShon et al*., 2003; *Newman et al*., 2002], lies beneath the Nicoya peninsula, making it an ideal site for multiple GPS campaigns and ocean-bottom seismometer deployments designed to investigate the seismic portion of the forearc and to identify regions associated with slow-slip, episodic tremor, and microseismicity [*Newman et al*., 2002; *Norabuena et al*., 2004; *Ghosh et al*., 2008; *Outerbridge et al*., 2010].

CNS-derived crust exhibits surface heat flow of 105–115 mW/m^2, consistent with conductive lithospheric cooling models for 18–24 Ma seafloor [*Parsons and Sclater*, 1977; *Stein and Stein*, 1994]. In contrast, the EPR crust is characterized by surface heat flow of only 20–40 mW/m^2 [*Langseth and Silver*, 1996; *Fisher et al*., 2003; *Harris et al*., 2010a, 2010b]. The sharp thermal transition and anomalously low heat flow is attributed to vigorous hydrothermal circulation through basaltic basement outcrops that provide a hydraulic connection between the igneous crust and the seafloor, resulting in efficient mining of heat by large-scale lateral fluid flow [*Fisher et al*., 2003; *Hutnak and Fisher*, 2007; *Harris et al*., 2010a, 2010b].

The thermal structure of the incoming plate has been well documented by >300 heat flow measurements conducted on both CNS and EPR-derived crust [*Fisher et al*., 2003; *Hutnak et al*., 2006; *Harris et al*., 2010a,

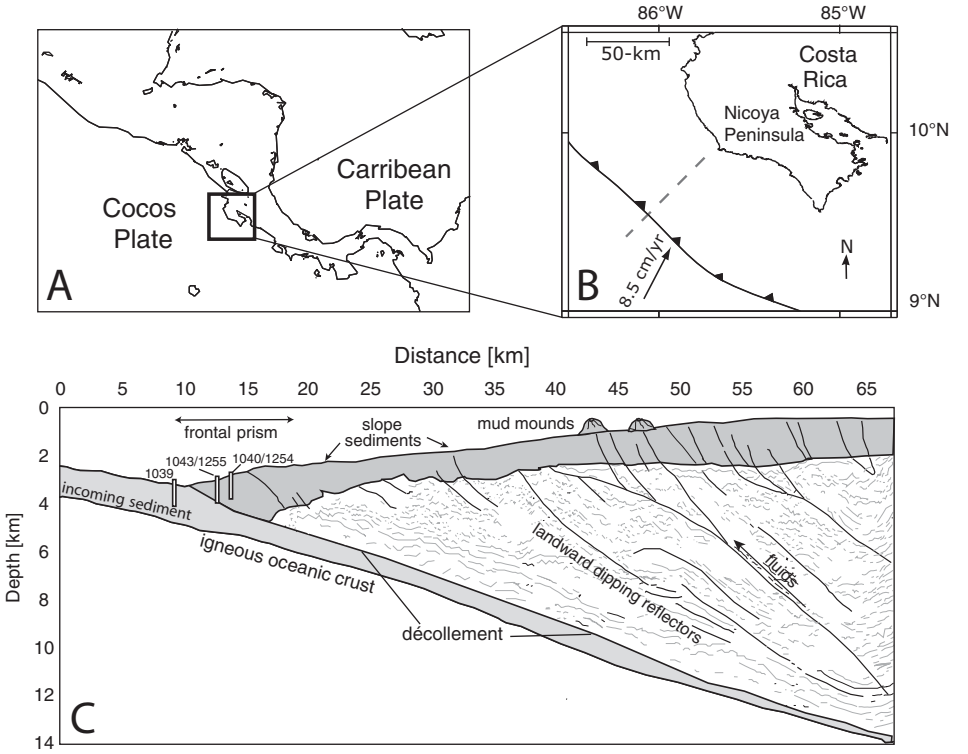

Figure 1. (a, b) Map of the study area, showing location of the subduction trench and the cross section and model transect (dashed line). (c) Interpreted cross section based on seismic reflection data, showing ODP drill sites and schematic locations of mud mounds (location shown by dashed line in Figure 1b [after *Hensen et al*., 2004; *Ranero et al*., 2008].

2010b], and the data have been used to parameterize 2-D thermal models of the subduction zone [e.g., *Harris and Wang*, 2002; *Spinelli and Saffer*, 2004]. These modeling studies show that the thermal structure of the subduction zone varies markedly along-strike. These variations may partly control pore pressure distribution and fluid flow patterns, by affecting the spatial distribution of both diagenetic fluid sources and fluid viscosity [*Spinelli and Saffer*, 2004].

The sediment on the incoming Cocos plate is approximately 400 m thick near Nicoya and consists of ~250 m of pelagic carbonate ooze underlying ~150 m of diatomaceous clay-rich mud [*Shipboard Scientific Party*, 1997a; *Spinelli and Underwood*, 2004]. Total sediment thickness decreases along-strike to the southeast, owing to changes in relief of the subducting plate associated with the Cocos Ridge, and also varies locally with basement topography [*Shipboard Scientific Party*, 2012a; *Harris et al*., 2012]. On average, the diatomaceous section contains ~60 wt % smectite, with no significant variation along strike [*Spinelli and Underwood*, 2004]. The total inventory of fluids entering the subduction zone is ~23.8 m^3/yr per m along strike, with 21.7 m^3 yr^{-1} present as pore fluid, and 2.1 m^3 yr^{-1} as bound water in hydrous (smectitic) clays. We do not consider fluid release from opal diagenesis here, as it represents only 0.4% of the total fluid inventory [*Spinelli and Saffer*, 2004; *Spinelli et al*., 2006].

The Nicoya region of the Costa Rican margin is nonaccretionary, meaning that all of the incoming sediment is subducted at the trench [e.g., *Shipley et al*., 1992; *Shipboard Scientific Party*, 1997b]. Apart from a small (~5 km wide) frontal prism composed of reworked slope sediments, the upper plate margin wedge consists primarily of basement rock, thought to be an extension of the onshore Nicoya Complex [*Kimura et al*., 1997; *Shipboard Scientific Party*, 1997b; *Vannucci et al*., 2001] (Figure 1). The wedge is overlain by a ~2.5 km thick drape of slope sediments, composed of clays, silts, and sands, and which is lithologically similar to the frontal prism [*Kimura et al*., 1997].

2.2. Forearc Hydrogeology

Several recent studies have investigated the hydrogeology of the Costa Rican forearc through a combination of ocean drilling, geophysical surveys, direct sampling of pore fluids in areas of focused flow, and

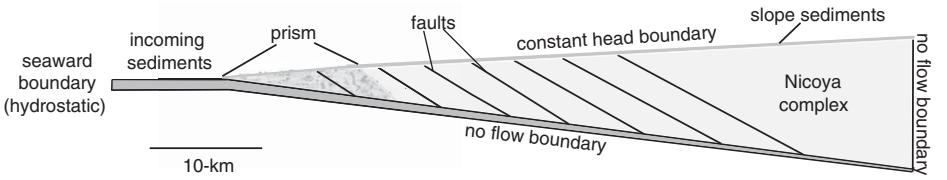

Figure 2. Diagram of model domain delineating subducting sediments (dark gray), margin wedge (light gray), frontal prism (stippled area), slope sediments, and splay faults and décollement (lines).

numerical modeling studies designed to quantify patterns of fluid flow, heat and chemical transport, and fluid budgets [e.g., *Shipley et al*., 1992; *Kimura et al*., 1997; *Silver et al*., 2000; *Cutillo et al*., 2003; *Hensen et al*., 2004; *Screaton and Saffer*, 2005; *Spinelli et al*., 2006; *Lauer and Saffer*, 2012; *Kluesner et al*., 2013]. Together, these studies afford a basic understanding of the outer forearc hydrogeology, where flow is primarily attributed to rapid compaction of the subducted sediments.

Pore waters characterized by low chlorinity and enrichment in thermogenic hydrocarbons and Li have been sampled from the décollement at IODP Sites 1040, 1043, and 1254, and in the overlying wedge at Sites 1043 and 1040 [*Shipboard Scientific Party*, 1997a; *Silver et al*., 2000; *Chan and Kastner*, 2000; *Shipboard Scientific Party*, 2003; *Spinelli et al*., 2006]. These fluid geochemical signatures are consistent with source temperatures of 60–160°C [*Chan and Kastner*, 2000], suggesting transport from ~20 to 25 km downdip and implying that the plate boundary is sufficiently permeable to transmit fluids from the site of these reactions to the trench. In addition, active seeps, in some cases characterized by low chloride fluids enriched in Boron and thermogenic hydrocarbons, have been documented at fault scarps and active mud mound structures on the upper slope that are associated with splay faults cutting the upper plate [e.g., *Hensen et al*., 2004; *Sahling et al*., 2008]. Geochemical and isotopic analyses suggest that the chemically distinct fluids originate at temperatures of 85–150°C.

3. Modeling Methods

We use the finite element code SUTRA [*Voss*, 1984] to simulate steady state fluid flow and solute transport along a 70 km transect oriented perpendicular to the trench [e.g., *Spinelli et al*., 2006; *Lauer and Saffer*, 2012] (Figures 1 and 2). A steady state simulation was chosen to represent the time-averaged, long-term flow rates and pathways [e.g., *Ranero et al*., 2008], and the fluid pressure distribution that develops in response to subduction. Simulated fluid pressures and flow are driven by two processes: (1) tectonic loading and subsequent compaction (porosity loss) of sediments on the incoming plate and (2) smectite transformation to illite [e.g., *Bekins and Dreiss*, 1992; *Bekins et al*., 1995; *Spinelli et al*., 2006].

Steady state fluid flow is described by

$$\nabla\left[\left(\frac{k\rho_w}{\mu}\right)\right]\cdot(\nabla P_f-\rho_w g)-\rho\Gamma=0, \tag{1}$$

where k is permeability (m^2), ρ_w is fluid density (kg m^{-3}), μ is dynamic fluid viscosity (Pa s), P_f is fluid pressure (Pa), and Γ ($V_{water}/V_{sediment/rock}$ s^{-1}) is a fluid source term that includes both compaction and clay transformation. Clay transformation introduces freshwater to the system; we use Chloride [Cl^-] as a conservative tracer to track the fate of these fluids [e.g., *Kastner et al*., 1991; *Bekins et al*., 1995]. Steady state nonreactive solute transport is described by

$$\nabla\cdot(v\rho_w C)-\nabla\cdot(D\nabla\rho_w C)=0, \tag{2}$$

where the first term describes the advective component of transport, where v is fluid velocity (m s^{-1}) and C is molal concentration, and the second term describes the diffusive component of transport, where D is the coefficient of hydrodynamic dispersion (m^2 s^{-1}).

Our model domain extends from 10 km seaward to 60 km landward of the trench and includes the upper plate and subducting sediments [e.g., *Spinelli et al*., 2006] (Figure 2). Based on constraints from seismic reflection data and drilling, we include a 2.5 km thick drape of slope sediments overlying the margin wedge, and a small (5 km wide) frontal prism composed of accreted and reworked slope sediment [*Kimura et al*.,

1997; *Silver et al*., 2000] (Figures 1 and 2). We define the model geometry using a taper angle of 11.4° (décollement dip, $\beta = 7.6°$; surface slope, $\alpha = 3.8°$), and a fault spacing of 5 km based on seismic reflection studies (Figures 1 and 2) [*Ranero et al*., 2008; *Shipley et al*., 1992].

The top and seaward edges of the model domain are set to a hydrostatic pressure (constant head boundary condition) and a seawater Cl^- concentration (550 mM). The bottom and landward edges of the domain are set to a no-flow boundary condition (Figure 2), assuming: (1) there is minimal hydraulic communication between the sediments and basaltic oceanic crust, as suggested by the estimated pore fluid pressure distribution within the subducting sediment section [e.g., *Saffer*, 2003] and (2) fluid sources >60 km from the trench are negligible [e.g., *Bekins et al*., 1995; *Spinelli et al*., 2006]. Previous studies have shown that including permeable upper oceanic crust has a small effect on simulated fluid fluxes and pore pressures, except when the sediments themselves are highly permeable [e.g., *Saffer and Bekins*, 1998; *Matmon and Bekins*, 2006], so relaxing the first assumption above would not appreciably impact our results.

We consider two scenarios for the margin thermal structure, to explore the range of dehydration-driven fluid sources and solute transport behaviors associated with warm and cold end-members [e.g., *Spinelli et al*., 2006]. We define these two cases based on heat flow studies and thermal modeling efforts along the Middle America Trench [*Harris et al*., 2010a, 2010b]. For the cold model, we incorporate a thermal structure consistent with low heat flow on the incoming EPR-derived crust ($Q = 30$ mW/m^2; equivalent to a geothermal gradient on the incoming plate of 12.5°C/km). For our warm model, we use a thermal structure consistent with the CNS-derived plate heat flow of 120 mW/m^2 (50°C/km). In all of our simulations, we account for the effect of temperature on fluid viscosity (μ) by

$$v = 2.4 \times 10^{-5}\left[10^{248.37/(T+133.15)}\right], \tag{3}$$

where temperature (T) is in degrees Celsius [*Voss*, 1984].

3.1. Porosity Distribution and Compaction-Driven Fluid Sources

We compute compaction-derived fluid sources from assumed porosity loss as sediments are transported into the subduction zone and progressively buried [e.g., *Bekins and Dreiss*, 1992; *Screaton et al*., 1990]. We fix our reference frame at the trench and consider the transport of sediments through a steady state porosity field that reflects compaction and porosity loss with depth and distance arcward of the deformation front [e.g., *Le Pichon et al*., 1990; *Screaton et al*., 1990; *Bekins and Dreiss*, 1992]. Because the Costa Rican margin is nonaccretionary, the compaction-driven fluid source terms arise only in subducted sediments. Under the assumption of uniaxial (vertical) consolidation and conservation of solid mass, fluid sources (Γ; V_{fluid}/V_{sed} s^{-1}) are given by [*Saffer*, 2003]

$$\Gamma = \frac{\partial \phi}{\partial z} \tan(\alpha + \beta) \cdot v_p, \tag{4}$$

where v_p is the plate convergence rate (m s^{-1}), ϕ is fractional porosity (unitless), and z is the depth below the seafloor (m).

We define porosity (ϕ) using a porosity-depth relationship that honors data from drilling at the Costa Rican margin (IODP Leg(s) 170, 205; Sites 1039, 1040, 1043; Figure 3), laboratory consolidation test results on core samples of both the pelagic and hemipelagic units [*Saffer*, 2003; *Screaton and Saffer*, 2005], and observations from exhumed subduction zone sedimentary rocks [e.g., *Bray and Karig*, 1985]. The compaction trends for the two lithologies are similar, and well fit by an exponential decay with depth (Figure 3) [e.g., *Athy*, 1930; *Bray and Karig*, 1985]

$$\phi(z) = 0.7136\, e^{-.3714 z} \quad 0 < z < 5000\,\text{m}, \tag{5a}$$

$$\phi(z) = 0.4\, e^{-.21 z} \quad z \geq 5000\,\text{m}. \tag{5b}$$

Porosity values range from >0.70 at the trench to 0.03 at a burial depth of 12.5 km (Figure 3).

3.2. Clay Dehydration Fluid Sources and Fluid Source Composition

The largest fluid source from mineral dehydration results from the transformation of smectite-group clay minerals to illite [*Moore and Vrolijk*, 1992], a reaction that occurs in a series of individual steps that are described

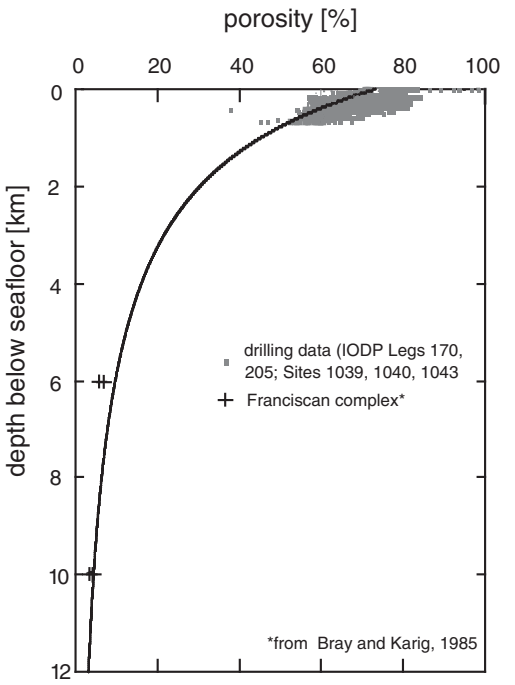

Figure 3. Porosity-depth trend described by equation (5) (solid black curve), based on data from shallow ODP and IODP drill holes (gray squares) [*Shipboard Scientific Party*, 1997a, 1997b, 1997e], and exhumed subduction zone sediments (crosses) [*Bray and Karig*, 1985].

well by a single "lumped" kinetic expression [e.g., *Pytte and Reynolds*, 1988; *Huang et al*., 1993]. Here we consider only smectite to illite transformation in the hemipelagic sediments, although there is likely additional fluid release at higher temperatures and greater depths (>~200°C) from the dehydration of Mg-smectites (saponite) formed by alteration of basaltic oceanic crust [e.g., *Staudigel et al*., 1981]. The porosity and temperature in the sedimentary section vary primarily as a function of burial depth, or distance from the trench, with no significant variation vertically within the section. As a result, the reaction progress and fluid production rates are also invariant in the *z* direction, and simulated smectite release is tied to the midpoint of the sedimentary section.

The reaction rate for illitization is determined primarily by the exposure time and temperature of the sediments, which are in turn controlled by the plate convergence rate and thermal structure [e.g., *Saffer et al*., 2008]. At Costa Rica, the thermal state of the incoming plate varies along strike, but the sediments are thin, and as a result, temperatures are not high enough to initiate reaction progress until ~20 km landward of the trench [*Spinelli et al*., 2006].

We use the kinetic expression of *Pytte and Reynolds* [1988] to describe the reaction, because it provides the best fit to the available data that cover the large range of temporal and thermal conditions experienced by subducted sediments, and matches observed reaction progress at other subduction zones well [*Bekins and Dreiss*, 1994; *Saffer et al*., 2008]. The reaction rate is given by

$$\frac{\partial S}{\partial t} = -Ae^{-E/RT}\left(\frac{[K^+]}{[Na^+]}\right)S^5, \tag{6}$$

where S is the mole fraction of smectite in mixed layer illite-smectite, A is a scaling factor (5.2×10^{-7} s^{-1}), E is activation energy (1.38×10^{-5} J mol^{-1}), R is the ideal gas constant, and T is temperature (Kelvin). As noted above, we define the temperature field from the results of a recent suite of thermal models for the Costa Rica margin [*Harris et al*., 2010a, 2010b].

We assume an end-member scenario in which all of the interlayer clay in the hemipelagic section is initially smectite ($S_{initial} = 1.0$). Analysis of the incoming sediment indicates a mean mole fraction of ~90% smectite ($S_{initial} = 0.90$) in the mixed-layer clays [*Spinelli and Underwood*, 2004]. In applying equation (6), we also assume that the ratio of K^+ to Na^+ is in equilibrium with K-feldspar [*Pytte and Reynolds*, 1988]

$$\left(\frac{[K^+]}{[Na^+]}\right) = 74.2\, e^{\frac{-2490}{T}}. \tag{7a}$$

The rate of fluid release from smectite transformation is given by

$$\Gamma_{illitization} = \frac{\partial S}{\partial t} \cdot H \cdot C \cdot (1-\phi), \tag{7b}$$

where H is the volumetric water content of smectite ($V_{H2O}/V_{smectite}$) and C is the volume fraction of smectite in the dry (solid fraction) bulk sediment, defined by the product of overall clay abundance in the sediment and smectite abundance in the clay fraction. We assume there are initially two layers of bound water in the smectite, corresponding to a volumetric water content (H) of 0.4 (15 Å d-spacing) [*Colten-Bradley*, 1987; *Bird*, 1984], and that C = 0.6, based on the XRD data [*Spinelli and Underwood*, 2004]. The calculated rate of fluid

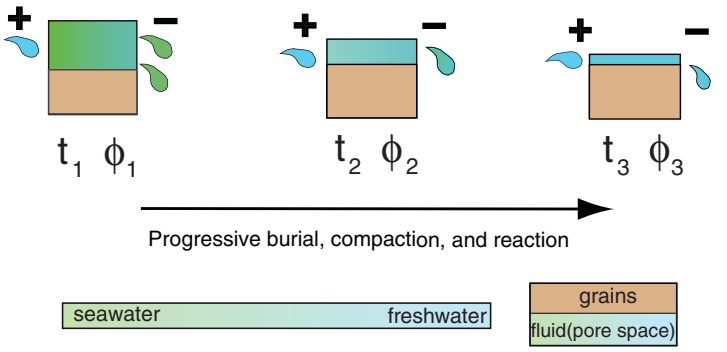

Figure 4. Schematic diagram illustrating mixing calculation for the chloride concentration of fluid source terms. The concentration of fluids within the subducting sediments, and which is expelled as the sediments are progressively buried, is defined by the mixing of freshwater released by smectite dehydration with extant pore fluid.

release does not explicitly represent distinct pulses from different layers of bound water [e.g., *Perry and Hower*, 1972] and assumes that fluid release occurs continuously and in parallel with the formation of illite crystallites [e.g., *Saffer et al.*, 2008].

Implicit in equation (7a) is the assumption that the reaction is not limited by K^+ availability. If we were to consider a case in which K^+ is a limiting factor in reaction progress [e.g., *Perry and Hower*, 1970], actual fluid production rates would be lower than we report, and the reaction would extend to greater depths. In our calculation of the source terms, we also assume that (1) any porosity increase caused by a decrease in the volume of solid phases during illitization collapses to remain on the compaction trend defined by equation (5) (Figure 3) [e.g., *Bekins et al.*, 1995; *Fulton et al.*, 2009] and (2) a 5% increase in volume of the interlayer water occurs upon expulsion [e.g., *Bethke*, 1986]. Taking these assumptions into account, along with our choice of $S_{initial} = 1.0$, the dehydration fluid source terms we report should be considered maxima.

To compute the chemistry (chlorinity) of fluid sources in our model domain, we track the composition of pore fluids as the sediments undergo consolidation and illitization. We accomplish this using a mixing model that accounts for porosity loss and progressive freshening from bound water release as sediments are transported landward with the subducting slab (Figure 4)

$$Cl^-_{i+1} = \frac{Cl^-_{i+1}\,\phi_i}{\phi_i + \Gamma_{illitization}\,dt}, \tag{8}$$

where the subscripts (i) and (i + 1) refer to a given location and a subsequent position downdip, the presubduction chloride concentration is set to a seawater value (550 mM), and *dt* is the time required for transport of the sediment to the new position.

3.3. Permeability Architecture

Consolidation leads to a corresponding decrease in permeability, with the highest rates of reduction occurring within the first 5 km of burial (Figure 5) [*Shipley et al.*, 1990; *Saffer et al.*, 2000; *Saito and Goldberg*, 2001]. We define the permeability of the incoming and subducted sediments using log linear permeability-porosity relationships similar to those used by *Spinelli et al.* [2006] in their regional hydrogeologic model of the margin, and which is defined by their detailed sensitivity analysis of modeled pore fluid pressure, in combination with laboratory measurements over a wide range of effective stresses on core samples from ODP Sites 1039, 1040, 1254, and 1255 [*Saffer and McKiernan*, 2005]

$$k(\phi) = 10^{-21.33+6.8874\phi} \quad \text{hemipelagic}, \tag{9a}$$

$$k(\phi) = 10^{-20.91+6.31\phi} \quad \text{pelagic}. \tag{9b}$$

We assign an effective vertical permeability of 2×10^{-17} m^2 to the 2.5 km thick section of slope sediments draping the upper plate, based on the porosity depth distribution defined by drilling, and laboratory-derived permeability-porosity relationships for similar slope sediments offshore Peru [*Marsters and Christian*, 1990]. Based on lithologic similarities identified during drilling [*Kimura et al.*, 1997], we assign the small frontal prism the same permeability as the slope sediments.

To explore the role of splay faults in partitioning of deeply sourced fluids and translating fluid pressures, we include seven faults that connect the décollement to the seafloor and cut across the upper plate

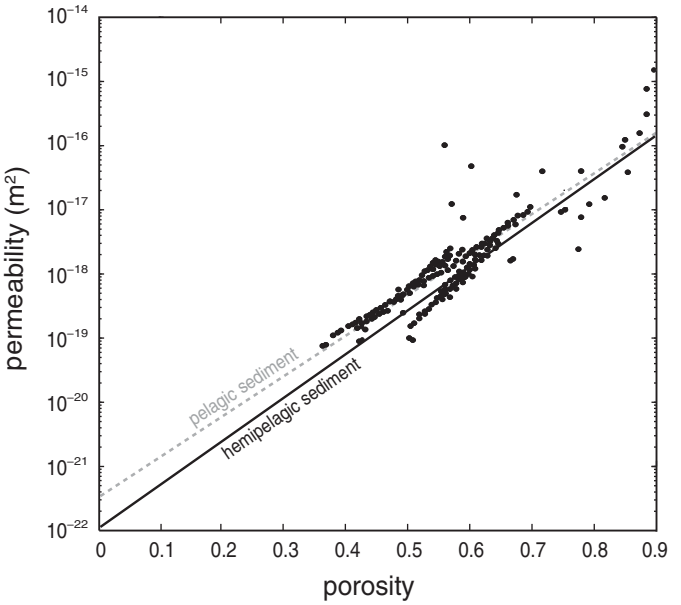

Figure 5. Experimentally determined porosity-permeability relationships for the hemipelagic mudstones sampled in drillsites at the Nicoya margin [*Saffer and McKiernan*, 2005]. The solid and dashed lines represent the porosity-permeability relationships used in the flow and transport model, and described in equations (9a) and (9b).

[*Lauer and Saffer*, 2012] (Figure 2). Based on seismic reflection surveys of the margin [*Ranero et al*., 2008; *Shipley et al*., 1992], we specify that the splay faults dip 30° landward and are spaced 5 km apart. We define a baseline model that includes a 60 m thick permeable décollement (10^{-14} m^2), a constant permeability for the upper plate (10^{-19} m^2), and without permeable splay faults (i.e., the splay fault permeabilities are set to 10^{-19} m^2, the same value as the surrounding rock of the upper plate). We then consider a range of splay fault permeabilities from 10^{-16} to 10^{-12} m^2; this range is based on previous sensitivity studies that indicate décollement permeability of 10^{-14} m^2 and splay fault permeabilities of 10^{-13} m^2 to 10^{-16} m^2 are most consistent with existing observations of flow rate, pore water geochemistry, and pore pressure [e.g., *Saffer and Screaton*, 2003; *Hensen et al*., 2004; *Ranero et al*., 2008; *Solomon et al*., 2009; *Lauer and Saffer*, 2012].

4. Results and Discussion

4.1. Reaction Progress and Fluid Sources

The transformation of smectite to illite is primarily controlled by the temperature field and exposure time, which are determined by the thermal state of the subduction zone and the convergence rate [e.g., *Saffer et al*., 2008]. In our simulations of a cold margin, illitization initiates 25 km from the trench, where temperatures reach ~60°C. In these models, fluid sources from dehydration exceed those from compaction by ~30 km from the trench (Figure 6). The reaction proceeds with progressive burial and exposure to higher temperatures, until fluid sources peak ~40 km from the trench and then begin to decline beyond ~45 km. The decline in fluid production corresponds with the reaction midpoint (i.e., where S = 0.5). The reaction rate slows further downdip as the reactant is depleted, but produces up to 4 times the fluid source estimated from compaction throughout the remainder of the model domain (to 60 km landward of trench, Figure 6b). The source concentration is identical to seawater ($[Cl^-] = 550$ mM) until the onset of reaction 25 km from the trench, where it is progressively freshened with increasing distance landward, achieving a minimum concentration of 50 mM (Figure 6c).

In our warm margin simulations, the onset of illitization occurs <10 km from the trench, and the reaction progresses rapidly, with peak fluid sources and the reaction midpoint located 10–12 km from the trench (Figures 6a and 6b). Illitization sources exceed those estimated from compaction from ~8 to 28 km from the trench, and progressively decline with distance landward. Pore water freshening is focused around the location of peak dehydration; chloride concentrations decline from seawater concentration to ~300 mM over a distance of 10 km, and remain at this value beyond ~25 km from the trench once the reaction has reached completion.

The impact of clay transformation on pore water freshening depends strongly on the interplay of porosity evolution and the distribution of bound water release. In our cold margin scenario, the reaction peaks at a depth of 8.8 km bsf (~42 km from the trench), where the porosity is only ~6%. In contrast, for our warm margin scenario, dehydration initiates shallower and closer to the trench where porosity remains >25%. As

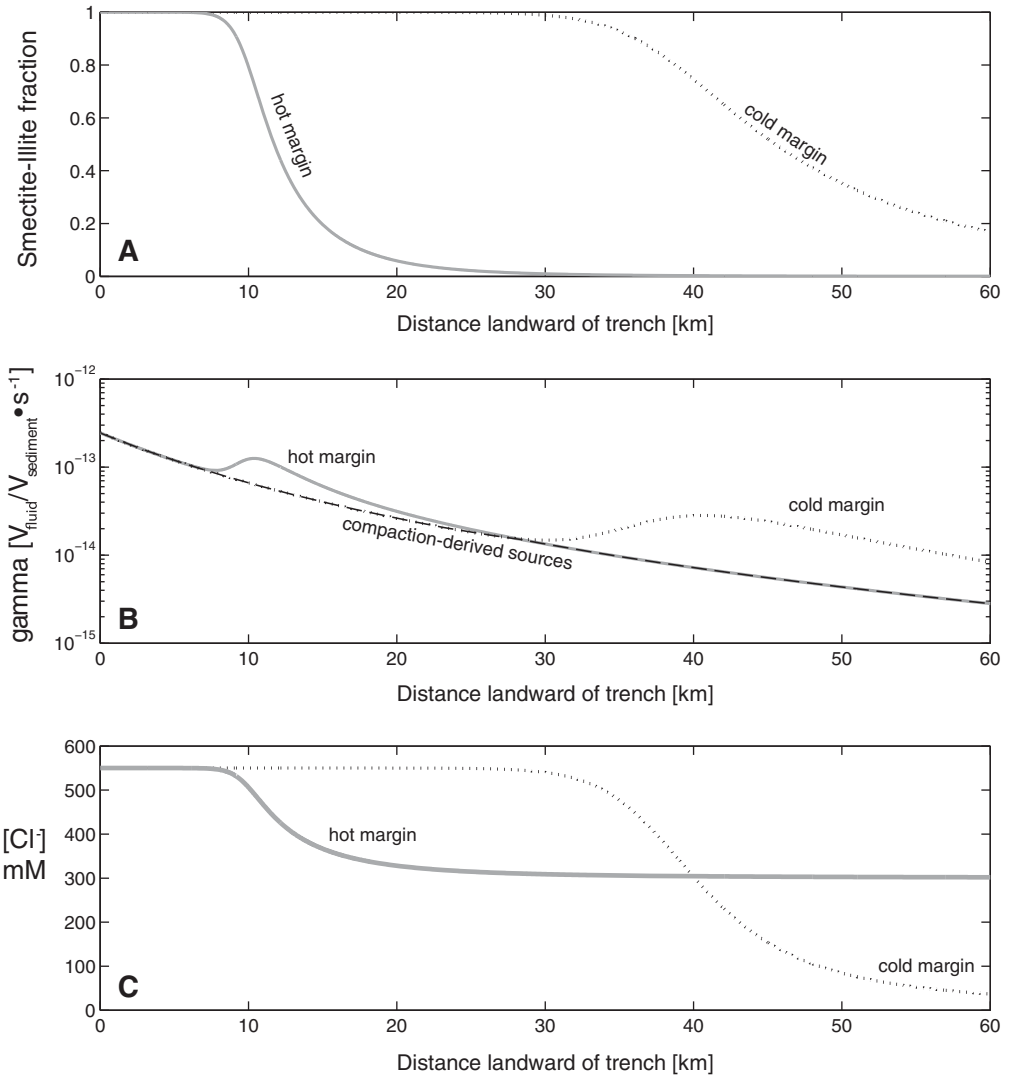

Figure 6. (a) Model results showing the progression of smectite transformation in the middle of the subducting sediment section. (b) Computed fluid source terms from compaction and clay dehydration. (c) Computed chloride concentration of fluid sources. In each figure, the solid and dashed lines represent our warm and cold margin scenarios, respectively.

a result, pore water freshening in the subducting section is diminished in the warm scenario, because clay transformation and the associated release of bound water occur at shallower depths and the dehydration-derived fluids are mixed with a larger volume of pore water.

It should be noted that we assign an average thickness (150 m) to the incoming hemipelagic section in our models, to assess the impact of differences in the thermal structure. Seismic reflection profiles and high-resolution bathymetry surveys of this region have identified many seamounts, and oceanic basement structures where the sediment is thin or absent [*Fisher et al*., 2003], which would lead to spatial variations in the smectite fluid source volume at the plate boundary. In our models, we track the clay transformation and pore water freshening in a column that is progressively buried and transported arcward, and use this as inputs for the 2-D flow model. As a result, variations in sediment thickness or stratigraphy would not change the strength, location, or concentration of dehydration-driven fluid sources in our models; it would simply make them "patchy," but the overall result remains robust to this kind of heterogeneity.

4.2. Splay Faults and Solute Transport

Our results show that splay faults effectively carry fluids away from their source at and below the plate boundary to the seafloor on the continental slope (Figure 7). The role of splay faults in intercepting fluids

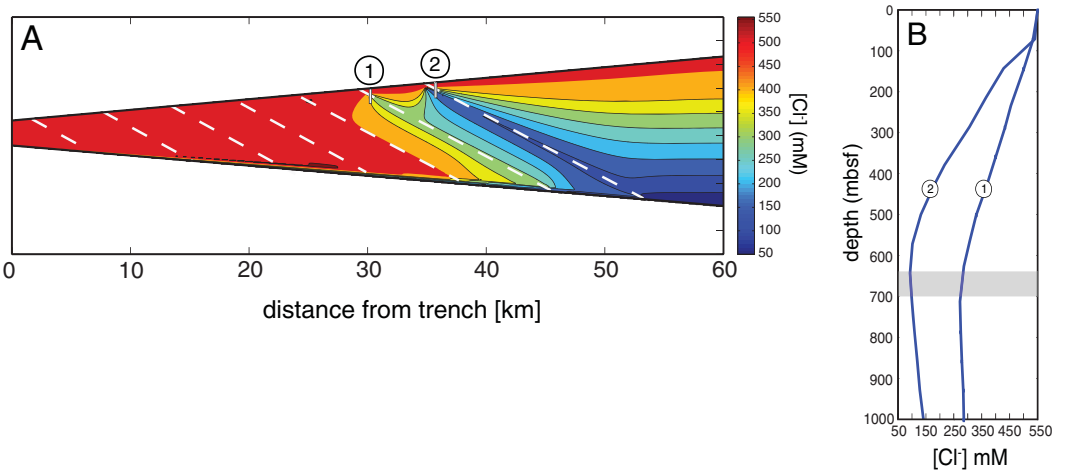

Figure 7. (a) Cross section showing simulated chloride concentrations for the case where $k_{decollement} = k_{faults} = 10^{-14}$ m^2. Geochemically distinct fluid from illitization is effectively intercepted by splay faults and carried to the seafloor landward of the trench. (b) Profiles of simulated pore water chlorinity across two faults on the slope (locations "1" and "2" shown on cross section), showing fault-centered low-Cl anomalies.

derived from clay dehydration, and therefore their effect on the distribution of pore fluid freshening through the forearc reflects an interplay between fault permeability and bound water release. The role of splay faults is amplified at cold margins, where pore fluid freshening occurs further from the trench—and is larger in magnitude than at warm margins—allowing deeply sourced fluids to be intercepted by conduits cutting the upper plate.

In our cold margin simulations, substantial freshening is limited to the region >30 km from the trench (Figures 6c and 7). The deeply sourced fluids are efficiently transmitted to the base of the slope sediments via the permeable splays, leading to fault-centered pore water freshening anomalies along those faults rooted at depths where substantial freshening has occurred (Figure 7). In contrast, splays tapping the subducting sediment and décollement <30 km from the trench are characterized by little or no pore water freshening, because dehydration is not a significant source of fluid in this region, and fluids sourced from greater depths are intercepted by the splay faults rather than flowing along the décollement to the trench. One key implication is that future drilling, coring, or submersible campaigns designed to sample deeply sourced fluids should focus on the mid to upper slope of the forearc, where permeable faults provide efficient flow paths to the seafloor.

Previous modeling studies have shown that faults also exert a strong control on the budget and partitioning of fluid egress between flow along the décollement, along splays, and exiting the forearc via diffuse flow, and that these effects scale with the permeability of the faults and décollement [*Lauer and Saffer*, 2012]. In our simulations, 18–33% of the total fluid inventory exits the forearc via splay faults, and the percentage increases systematically as k_{fault} is increased from 10^{-16} to 10^{-12} m^2 [*Lauer and Saffer*, 2012]. Of the remaining fluids, 38–60% exit along the décollement, and 29–31% exits diffusely through the frontal prism, primarily due to leakage from the décollement in the outer few kilometers of the system. The overall budget is largely insensitive to the margin thermal state, though slightly more fluid exits through splay faults in our cold scenario—and less along the décollement—owing to the shift in locus of fluid release from clay transformation (Figure 8a). For example, for our simulations of a cold margin and with $k_{fault} = 10^{-14}$ m^2, 38% of the total fluid source exits the fore ac along the décollement, with the remaining fluid transmitted via faults (33%) and diffuse flow through the prism and upper plate (29%) (Table 1). In our warm margin scenario, the illitization source is near the trench, and fluid fluxes along faults are reduced slightly, to 31% of the total source, with 38 and 31% of the fluid transmitted via the décollement and diffuse flow, respectively.

Interestingly, our results indicate that fault permeability does not have a similarly significant effect on solute transport. Modeled chloride concentrations of fluids exiting the forearc along splay faults are insensitive to splay fault permeability. Therefore, we report on fluid budgets for illitization-derived fluids for a single set of simulations in which $k_{fault} = k_{decollement} = 10^{-14}$ m^2 (Table 1). In our cold margin scenario, dehydration-derived fluids exit the forearc primarily along faults (64%), with the remaining 36% exiting the forearc

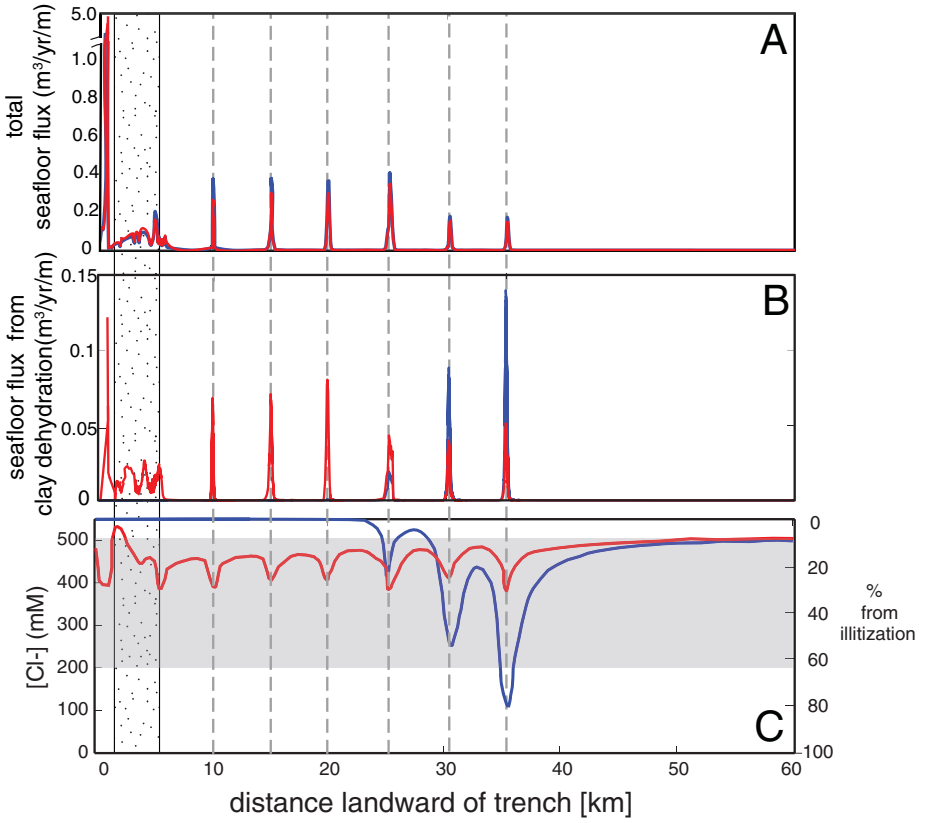

Figure 8. Fluid fluxes and chlorinities for our warm (red line) and cold (blue line) margin simulations, for the case where $k_{decollement} = k_{faults} = 10^{-14}$ m^2. (a) Total fluxes at the seafloor (m^3 fluid per m along strike); (b) fluxes of fluid derived exclusively from smectite transformation; and (c) chloride concentration of fluids exiting the forearc (mM), also shown as the percentage of the fluid derived from clay transformation (right axis), with the gray shaded region illustrating the projected location and range of chlorinity documented at mud mounds by *Hensen et al.* [2004]. The stippled region delineates the extent of the frontal prism.

diffusely through the upper plate, and none exiting along the décollement or through the frontal wedge (Figure 8b and Table 1). Because fluid release from illitization is shifted closer to the trench in the warm scenario, the partitioning of these fluids is also shifted; 50% exits the forearc via the décollement, and only 21% is transmitted along splay faults (Table 1). The remaining fluid exits diffusely through the frontal prism (26%) and Nicoya complex (3%) (Figure 8 and Table 1).

In our cold margin models, fluids exiting faults >25 km from the trench are significantly depleted in chloride, with values as low as 100 mM [Cl^-] (~18% of seawater) (Figure 8c). Fluids exiting within 25 km of the trench, however, have a seawater composition, because all of the deeply sourced fluids have been effectively translated to the seafloor via the more landward splay faults that root where the dehydration reaction peaks [e.g., *Ranero et al.*, 2008]. In our warm margin models, fluids exiting along faults are freshened even at the trench, and the chloride concentrations of fluids exiting the system remain between 300 and 400 mM across the forearc (Figure 8c).

Table 1. Summary of Fluid Budget for Simulations of a Warm and Cold Margin with $k_{decollement} = k_{faults} = 10^{-14}$m^2

	Exits Forearc via	% Warm Margin	% Cold Margin
Total fluid source	Faults	31	33
	Décollement	38	38
	Diffuse	31	29
Illitization source	Faults	21	64
	Décollement	50	0
	Diffuse	29	36

Geochemical sampling of fluids venting from mound structures on the upper slope offshore Costa Rica document a strong signature of deeply sourced dehydration reactions [*Hensen et al.*, 2004]. The mound fluids are consistently depleted in chloride, with concentrations between 200 and 500 mM, similar to that of fluids exiting faults in our models, especially in our cold margin scenario. More broadly, our results are consistent with observations from other subduction margins (both accretionary and nonaccretionary) that document progressive freshening of pore

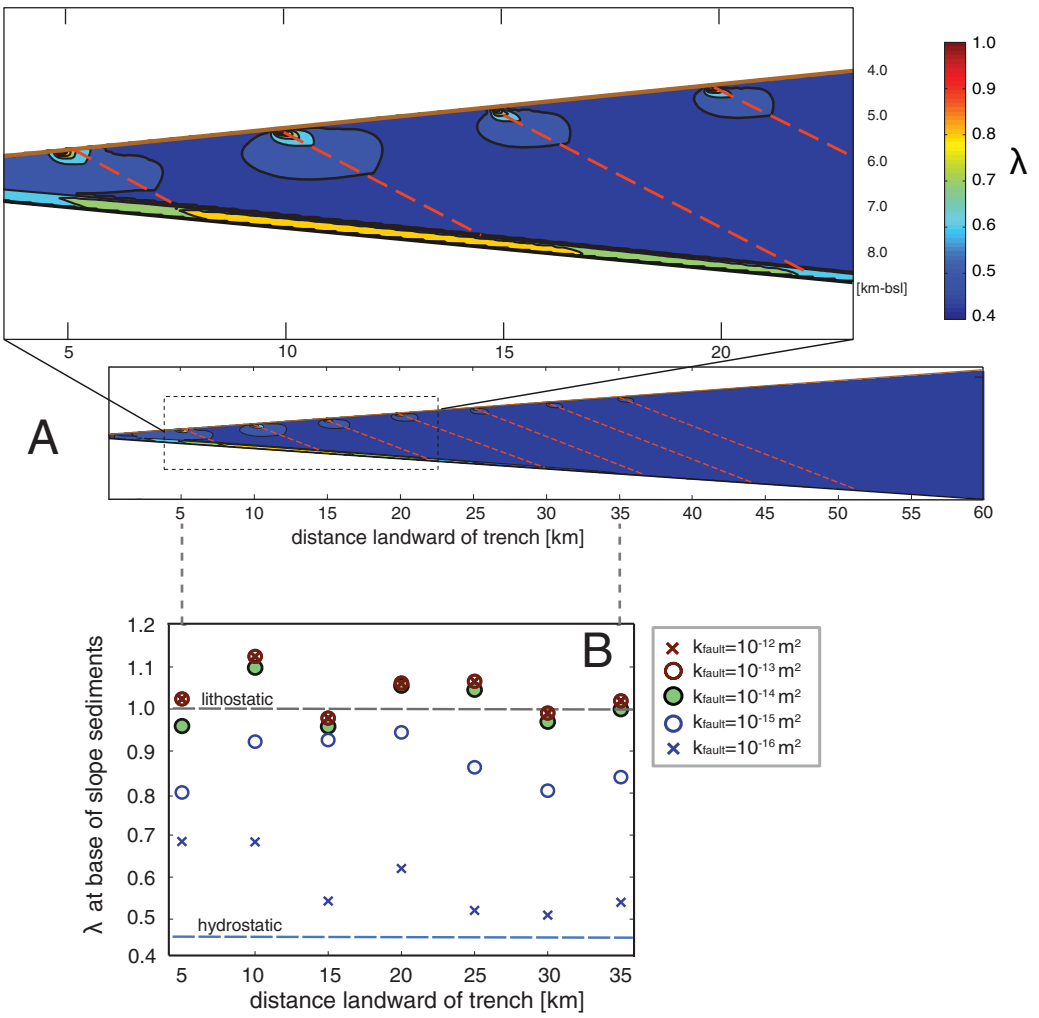

Figure 9. (a) Modeled pore pressure distribution throughout the model domain. Inset shows detail of region 3–23 km from the trench. (b) Modeled overpressure at the top of the faults where they intersect the base of the slope sediments, for a range of k_{faults} as noted, and with $k_{decollement} = 10^{-14}$ m^2. Value of λ equivalent to hydrostatic pressure is shown for reference (blue dashed line).

fluids sampled at the seafloor and in boreholes with distance from the trench. For example, in northeast Japan, freshened fluids with chlorinities of <300 mM (<50% of seawater) have been sampled within fractured zones in boreholes on the continental slope. The pore water freshening is attributed to clay dehydration at depth and subsequent transport through the upper plate along faults and fractures [*Kopf et al.*, 2003]. Similarly, at the Cascadia margin offshore Oregon, pore water geochemical data from ODP and IODP boreholes defines a trend of increasing diagenetic and metamorphic contribution with distance landward of the trench [*Torres et al.*, 2004; *Teichert et al.*, 2005]. An additional implication is that evidence of focused fluid expulsion along out of sequence and splay thrusts in the geologic record (exhumed subduction systems) may be best interpreted in this context and have served as preferential pathways for highly altered/chemically distinct fluids preserved in vein systems [*Rowe et al.*, 2005; *Yamaguchi et al.*, 2011].

4.3. Pore Pressure Distribution

As part of our analysis, we also explore the role of splay faults on pore pressure distribution and in translating fluid pressures updip. We report simulated pore pressures in terms of the overpressure ratio (λ)

$$\lambda = \frac{P_f}{P_l}, \tag{10}$$

where P_f is the fluid pressure and P_l is the lithostatic pressure. Our models do not explicitly include a feedback for permeability changes resulting from pressures that exceed lithostatic values, which would lead to

hydraulic fracture and permeability enhancement. In the case of hydraulic fracture, we expect that the associated permeability increase would valve fluid pressures, resulting in pressures that are dynamically maintained at or near lithostatic values [*Fulton et al*., 2009].

Modeled fluid pressures along and beneath the décollement do not exceed lithostatic, except in simulations with both fault and décollement permeabilities $<10^{-15}$ m^2 (Figure 9a). The highest overpressure ratio occurs ~12 km from the trench, where $\lambda = 0.87$, with a second region of elevated pressure ~40 km from the trench, localized in the pelagic sediment ($\lambda = 0.57$). The second peak corresponds with the location of peak clay transformation, where the dehydration fluid sources exceed those from compaction (cf. Figure 6). The impact of these reactions on fluid pressure is amplified at cold margins, because the reaction occurs in sediments with greatly diminished porosity and permeability.

We also find that overpressures are strongly focused at the base of the slope sediments, where splay faults about the overlying less permeable slope sediments (Figure 9). Pore pressures at the base of the slope sediment exceed hydrostatic values in all of our simulations (Figure 9). In simulations where $k_{fault} \geq k_{decollement}$, the simulated pore pressures are near or exceed lithostatic values ($\lambda = 1.0$). In cases where $k_{fault} \leq k_{décollement}$, pressures are lower, and increase systematically with increased splay fault permeability. The systematic variations in pressure translation with splay fault permeability are consistent with previous work showing that increased splay fault permeability results in greater capture of fluids at depth that would otherwise be channeled along the décollement or seep out of the system diffusely [*Lauer and Saffer*, 2012], and with the idea that higher permeability should lead to smaller head losses along the conduit. The translation and trapping of pressure along permeable structures or stratigraphic conduits has also been documented in other environments, and is known as the "centroid effect" [e.g., *Dugan and Flemings*, 2000; *Flemings et al*., 2002].

High fluid pressures are considered the dominant mechanism in the formation of mud volcanoes, and their submarine occurrence is localized primarily in regions of tectonic compression or high sedimentation rates. The formation of these structures requires a thick package of high porosity, fine-grained, soft, uncompacted sediments [*Dimitrov*, 2002], similar to the slope sediments that blanket the upper slope offshore Costa Rica [*Shipley et al*., 1990]. Our results suggest a potential mechanism for the formation of a piercement structure where transmissive faults translate pressures updip to the base of the thick slope sediment package [*Milkov*, 2000; *Dimitrov*, 2002]. This is consistent with observations at Costa Rica, where (1) mud mounds are most common on the mid to upper slope [*Shipley et al*., 1990] and (2) the geochemical signature of exiting fluids suggests a hydraulic connection all the way to the plate boundary below [*Hensen et al*., 2004].

5. Summary

Our results highlight the role of splay faults in effectively transmitting the geochemical signature of deeply sourced dehydration reactions to the seafloor, and in translating fluid pressures from the plate boundary to the base of the slope sediments. Differences in thermal structure determine the locus of clay transformation, and thus play a key role in the extent of freshening, and ultimately the distribution of freshened fluids in the forearc, by controlling the composition of fluids accessed by faults rooted at the plate interface.

The results are consistent with observations at fluid seeps and regions of focused flow on the upper slope [e.g., *Hensen et al*., 2004; *Ranero et al*., 2008; *Lauer and Saffer*, 2012]. Splay faults effectively tap into the zone of peak freshening, especially where the hydraulic impedance is less than that along the décollement to the trench. Faults that intercept the slope within 25 km of the trench transmit 27% of the total fluid inventory while those farther landward transmit only 4–6% of the fluid sources. The fate of dehydration-derived fluids is strongly dependent on thermal structure, and largely independent of fault permeability. In our cold scenario, 64% of dehydration-derived fluids are intercepted by splay faults and carried to the middle and upper slope; in the warm scenario, dehydration sources peak close to the trench, and faults transmit only 21% of these fluids, and the fluids they access are not as depleted in Cl^-, and exhibit a weaker signal of freshening. This modeled distribution of deeply sourced fluid is also consistent with observations of depleted chloride with distance landward from the trench at other subduction zones [e.g., *Kopf et al*., 2003; *Bekins et al*., 1994; *Torres et al*., 2004] and provides a context for interpreting evidence of focused fluid expulsion in exhumed subduction systems [*Rowe et al*., 2005; *Yamaguchi et al*., 2011]. Another key implication is that future efforts to sample deeply sourced fluids by drilling or seafloor campaigns should focus on clearly imaged faults along the mid to upper slope, rather than the trench. Where faults intersect the slope sediments, near-lithostatic pressures

develop at the base of the sediments, as fluid pressures are translated along the dipping faults (Figure 9). We suggest that this is a mechanism for the generation of mud volcanoes and mud mounds and can explain their association with both seepage of deeply sourced fluids and the locations of splay faults.

Acknowledgments
The drilling data used to parameterize models in this study can be accessed through the central ODP/IODP data portal, or Scientific Earth Drilling Information Service (sedis.iodp.org/). This work was supported by NSF awards 0503905, 0648331, and 0752114 to D.S. We thank Rob Harris and Barbara Bekins for their comments and discussions that improved this study.

References

Athy, L. F. (1930), Density, porosity, and compaction of sedimentary rocks, *Am. Assoc. Pet. Geol. Bull.*, *14*, 1–24.
Barkhausen, U., C. Renaro, R. von Huene, S. C. Cande, and H. A. Roeser (2001), Revised tectonic boundaries in the Cocos Plate off Costa Rica: Implications for the segmentation of the convergent margin and for plate tectonic models, *J. Geophys. Res.*, *106*(B9), 19,207–19,220.
Bekins, B. A., and S. J. Dreiss (1992), A simplified analysis of parameters controlling dewatering in accretionary prisms, *Earth Planet. Sci. Lett.*, *109*(3), 275–287.
Bekins, B. A., and S. J. Dreiss (1994), Influence of kinetics on the smectite to illite transition in the Barbados accretionary prism, *J. Geophys. Res.*, *99*(B9), 18,147–18,158, doi:10.1029/94JB01187.
Bekins, B. A., A. M. McCaffrey, and S. J. Dreiss (1995), Episodic and constant flow models for the origin of low-chloride waters in a modern accretionary complex, *Water Resour. Res.*, *31*(12), 3205–3215.
Bell, R., R. Sutherland, D. H. Barker, S. Henrys, S. Bannister, L. Wallace, and J. Beavan (2010), Seismic reflection character of the Hikurangi subduction interface, New Zealand, in the region of repeated Gisborne slow slip events, *Geophys. J. Int.*, *180*(1), 34–48.
Bethke, C. M. (1986), Inverse hydrogeologic analysis of the distribution and origin of Gulf Coast–type geopressured zones, *J. Geophys. Res.*, *91*(B6), 6535–6545.
Bird, P. (1984), Hydration-phase diagrams and friction of montmorillonite under laboratory and geologic conditions, with implicaions for shale compaction, slope stability, and strength of fault gouge, *Tectonophysics*, *107*, 235–260.
Bray, C. J., and D. E. Karig (1985), Porosity of sediments in accretionary prisms and some implications for dewatering processes, *J. Geophys. Res.*, *90*(B1), 768–778.
Byerlee, J. (1990), Friction, overpressure, and fault normal compression, *Geophys. Res. Lett.*, *17*(12), 2109–2112.
Chan, L. H., and M. Kastner (2000), Lithium isotopic compositions of pore fluids and sediments in the Costa Rica subduction zone: Implications for fluid processes and sediment contribution to the arc volcanoes, *Earth Planet. Sci. Lett.*, *183*(1), 275–290.
Colten-Bradley, V. A. (1987), Role of pressure in smectite dehydration: effects on geopressures and smectite-to-illite transformation, *Am. Pet. Geol. Bull.*, *71*, 1414–1427.
Cutillo, P. A., E. J. Screaton, and S. Ge (2003), Three-dimensional numerical simulation of fluid flow and heat transport within the Barbados Ridge accretionary complex, *J. Geophys. Res.*, *108*(B12), 2555, doi:10.1029/2002JB002240.
DeMets, C. (2001), A new estimate for Cocos-Caribbean plate motion: Implications for slip along the Central American volcanic arc, *Geophys. Res. Lett.*, *28*(21), 4043–4046.
DeShon, H. R., S. Y. Schwartz, S. L. Bilek, L. M. Dorman, V. Gonzalez, J. M. Protti, E. R. Flueh, and T. H. Dixon (2003), Seismogenic zone structure of the southern Middle America Trench, Costa Rica, *J. Geophys. Res.*, *108*(B10), 2491, doi:10.1029/2002JB002294.
Dimitrov, L. (2002), Mud volcanoes: The most important pathway for degassing deeply buried sediments, *Earth Sci. Rev.*, *59*(1), 49–76.
Dugan, B., and P. B. Flemings (2000), Overpressure and fluid flow in the New Jersey continental slope: Implications for slope failure and cold seeps, *Science*, *289*(5477), 288–291.
Expedition 334 Scientists (2012), Expedition 334 summary, in *Proceedings of Integrated Ocean Drilling Program*, vol. 334, edited by P. Vannucchi et al., Integrated Ocean Drill. Program Manage. Int. Inc., Tokyo, doi:10.2204/iodp.proc.334.101.2012.
Fisher, A. T., et al. (2003), Hydrothermal recharge and discharge across 50 km guided by seamounts on a young ridge flank, *Nature*, *421*(6923), 618–621.
Flemings, P. B., B. B. Stump, T. Finkbeiner, and M. Zoback (2002), Flow focusing in overpressured sandstones: theory, observations, and applications, *Am. Journal of Science*, *302*, 827–855.
Freed, R. L., and D. R. Peacor (1989), Variation in temperature of the Smectite/Illite reaction in Gulf Coast sediment, *Clay Miner.*, *24*, 171–180.
Freed, R. L., and D. R. Peacor (1992), Diagenesis and the formation of authigenic Illite-rich I/S crystals in Gelf-coast shales-TEM study of clay separates, *J. Sediment. Petrol.*, *62*(2), 220–234.
Fulton, P. M., D. M. Saffer and B. A. Bekins (2009), A critical evaluation of crustal dehydration as the cause of an overpressured and weak San Andreas Fault, *Earth Planet. Sci. Lett.*, *284*(3), 447–454.
Ghosh, A., A. V. Newman, A. M. Thomas, and G. T. Farmer (2008), Interface locking along the subduction megathrust from *b*-value mapping near Nicoya Peninsula, Costa Rica, *Geophys. Res. Lett.*, *35*, L01301, doi:10.1029/2007GL031617.
Harris, R., A. Sakaguchi, and K. Petronotis (2012), Costa Rica Seismogenesis Project, Program A Stage 2 (CRISP-A2): Sampling and quantifying lithologic inputs and fluid inputs and outputs of the seismogenic zone, Integrated Ocean Drill. Program Sci. Prosp., 344, doi:10.2204/iodp.sp.344.2012, p. 1–76.
Harris, R. N., and K. Wang (2002), Thermal models of the Middle America Trench at the Nicoya Peninsula, Costa Rica, *Geophys. Res. Lett.*, *29*(21), 2010, doi:10.1029/2002GL015406.
Harris, R. N., I. Grevemeyer, C. R. Ranero, H. Villinger, U. Barckhausen, T. Henke, C. Mueller, and S. Neben (2010a), Thermal regime of the Costa Rican convergent margin: 1. Along-strike variations in heat flow from probe measurements and estimated from bottom-simulating reflectors, *Geochem. Geophys. Geosyst.*, *11*, Q12S28, doi:10.1029/2010GC003272.
Harris, R. N., G. Spinelli, C. R. Ranero, I. Grevemeyer, H. Villinger, and U. Barckhausen (2010b), Thermal regime of the Costa Rican convergent margin: 2. Thermal models of the shallow Middle America subduction zone offshore Costa Rica, *Geochem. Geophys. Geosyst.*, *11*, Q12S29, doi:10.1029/2010GC003273.
Henry, P. (2000), Fluid flow at the toe of the Barbados accretionary wedge constrained by thermal, chemical, and hydrogeologic observations and models, *J. Geophys. Res.*, *105*(B11), 25,855–25,872.
Hensen, C., K. Wallmann, M. Schmidt, C. Ranero, and E. Suess (2004), Fluid expulsion related to mud extrusion off Costa Rica—A window to the subducting slab, *Geology*, *32*(3), 201–204.
Huang, W. L., J. M. Longo, and D. R. Pevear (1993), An experimentally derived kinetic model for smectite-to-illite conversion and its use as a geothermometer, *Clays Clay Miner.*, *41*, 162–177.
Hutnak, M., and A. T. Fisher (2007), Influence of sedimentation, local and regional hydrothermal circulation, and thermal rebound on measurements of seafloor heat flux, *J. Geophys. Res.*, *112*, B12101, doi:10.1029/2007JB005022.

Hutnak, M., A. T. Fisher, L. Zuehlsdorff, V. Speiss, P. H. Stauffer, and C. W. Gable (2006), Hydrothermal recharge and discharge guided by basement outcrops on 0.7-3.6 Ma seafloor east of the Juan de Fuca Ridge: Observations and numerical models, *Geochem. Geophys. Geosyst.*, *7*, Q07O02, doi:10.1029/2006GC001242.

Kastner, M., H. Elderfield, and J. B. Martin (1991), Fluids in convergent margins: What do we know about their composition, origin, role in diagenesis and importance for oceanic chemical fluxes, *Philos. Trans. R. Soc. London A*, *335*(1638), 243–259, doi:10.1098/rsta.1991.0045.

Kastner, M., H. Elderfield, W. J. Jenkins, J. M. Gieskes, and T. Gamo (1993), Geochemical and isotopic evidence for fluid flow in the western Nankai subduction zone, Japan, *Proc Ocean Drill Program Sci. Results*, *131*, 397–413.

Kimura, G., E. Silver, P. Bluma, and Shipboard Scientific Party (1997), in *Proceedings of Ocean Drilling Program Initial Reports*, vol. 170, pp. 1–554, Ocean Drill. Program, College Station, Tex.

Kitajima, H., and D. M. Saffer (2012), Elevated pore pressure and anomalously low stress in regions of low frequency earthquakes along the Nankai Trough subduction megathrust, *Geophys. Res. Lett.*, *39*, L23301, doi:10.1029/2012GL053793.

Kluesner, J. W., E. A. Silver, N. L. Bangs, K. D. McIntosh, J. Gibson, D. Orange, and R. Huene (2013), High density of structurally controlled, shallow to deep water fluid seep indicators imaged offshore Costa Rica, *Geochem. Geophys. Geosyst.*, *14*, 519–539, doi:10.1002/ggge.20058.

Kodaira, S., T. Iidaka, A. Kato, J. O. Park, T. Iwasaki, and Y. Kaneda (2004), High pore fluid pressure may cause silent slip in the Nankai Trough, *Science*, *304*, 1295–1298.

Kopf, A., G. Mora, A. Deyhle, S. Frape, and R. Hesse (2003), Fluid geochemistry in the Japan Trench forearc (ODP Leg 186): A synthesis, in *Proceedings of Ocean Drilling Program, Scientific Results*, vol. 186, edited by K. Suyehiro et al., pp. 1–23, Ocean Drill. Program, College Station, Tex.

Langseth, M. G., and E. A. Silver (1996), The Nicoya convergent margin—A region of exceptionally low heat flow, *Geophys. Res. Lett.*, *23*(8), 891–894.

Lauer, R. M., and D. M. Saffer (2012), Fluid budgets of subduction zone forearcs: The contribution of splay faults, *Geophys. Res. Lett.*, *39*, L13604, doi:10.1029/2012GL052182.

Le Pichon, X., P. Henry, and S. Lallemant (1990), Water flow in the Barbados accretionary complex, *J. Geophys. Res.*, *95*, 8945–8967.

Liu, Y., and J. R. Rice (2007), Spontaneous and triggered aseismic deformation transients in a subduction fault model, *J. Geophy. Res.*, *112*, B09404, doi:10.1029/2007/B004930.

Marsters, J. C., and H. A. Christian (1990), Hydraulic conductivity of diatomaceous sediment from the Peru continental margin obtained during ODP Leg 112, in *Proceedings of the Ocean Drilling Program, Scientific Results*, vol. 112, edited by E. Suess et al., pp. 633–638, Ocean Drill. Program, College Station, Tex.

Matmon, D., and B. Bekins (2006), Hydromechanics of a high taper angle, low-permeability prism: A case study from Peru, *J. Geophys. Res.*, *111*, B07101, doi:10.1029/2005JB003697.

Milkov, A. V. (2000), Worldwide distribution of submarine mud volcanoes and associated gas hydrates, *Mar. Geol.*, *167*, 29–42.

Moore, J. C., and D. Saffer (2001), Updip limit of the seismogenic zone beneath the accretionary prism of southwest Japan: An effect of diagenetic to low-grade metamorphic processes and increasing effective stress, *Geology*, *29*, 183–186.

Moore, J. C., and P. Vrolijk (1992), Fluids in accretionary prisms, *Rev. Geophys.*, *30*(2), 113–135.

Newman, A. V., S. Y. Schwartz, V. Gonzalez, H. R. DeShon, J. M. Protti, and L. Dorman (2002), Along-strike variability in the updip limit of the seismogenic zone below Nicoya Peninsula Costa Rica, *Geophys. Res. Lett.*, *29*(20), 1977, doi:10.1029/2002GL015409.

Norabuena, E., et al. (2004), Geodetic and seismic constraints on some seismogenic zone processes in Costa Rica, *J. Geophys. Res.*, *109*, B11403, doi:10.1029/2003JB002931.

Outerbridge, K. C., T. H. Dixon, S. Y. Schwartz, J. I. Walter, M. Protti, V. Gonzalez, J. Biggs, M. Thorwart, and W. Rabbel (2010), A tremor and slip event on the Cocos-Caribbean subduction zone as measured by a global positioning system (GPS) and seismic network on the Nicoya Peninsula, Costa Rica, *J. Geophys. Res.*, *115*, B10408, doi:10.1029/2009JB006845.

Parsons, B., and J. G. Sclater (1977), An analysis of the variation of ocean floor bathymetry and heat flow with age, *J. Geophys. Res.*, *82*(5), 803–827.

Peacock, S. M. (2009), Thermal and metamorphic environment of subduction zone episodic tremor and slip, *J. Geophys. Res.*, *114*, B00A07, doi:10.1029/2008JB005978.

Perry, E., and J. Hower (1970), Burial disgenesis in Gulf Coast pelitic sediments, *Clays and Clay Minerals*, *18*, 165–177.

Perry, E. A., Jr., and J. Hower (1972), Late-stage dehydration in deeply buried pelitic sediments, *Am. Assoc. Pet. Geol. Bull.*, *56*(10), 2013–2021.

Protti, M., V. Gonzalez, A. V. Newman, T. H. Dixon, S. Y. Schwartz, J. S. Marshall, L. Feng, J. I. Walter, R. Malservisi, and S. E. Owen (2014), Nicoya earthquake rupture anticipated by geodetic measurement of the locked plate interface, *Nat. Geosci.*, *7*(2), 117–121, doi:10.1038/ngeo2038.

Pytte, A. M., and R. C. Reynolds (1988), The thermal transformation of smectite to illite, in *Thermal History of Sedimentary Basins*, edited by N. D. Naeser and T. H. McCulloh, pp. 133–140, Springer, Berlin.

Ranero, C. R., I. Grevemeyer, H. Sahling, U. Barckhausen, C. Hensen, K. Wallmann, W. Weinrebe, P. Vannucchi, R. von Huene, and K. McIntosh (2008), Hydrogeological system of erosional convergent margins and its influence on tectonics and interplate seismogenesis, *Geochem. Geophys. Geosyst.*, *9*, Q03S04, doi:10.1029/2007GC001679.

Reyners, M., and D. Eberhart-Phillips (2009), Small earthquakes provide insight into plate coupling and fluid distribution in the Hikurangi subduction zone, New Zealand, *Earth Planet. Sci. Lett.*, *282*(1–4), 299–305, doi:10.1016/j.epsl.2009.03.034.

Rowe, C., J. C. Moore, F. Meneghini, and A. McKeirnan (2005), Large-scale pseudotachylytes and fluidized cataclasites from an ancient subduction thrust fault, *Geology*, *30*(12), 937–940.

Saffer, D. M. (2003), Pore pressure development and progressive dewatering in underthrust sediments at the Costa Rican subduction margin: Comparison with northern Barbados and Nankai, *J. Geophys. Res.*, *108*(B5), 2261, doi:10.1029/2002JB001787.

Saffer, D. M., and B. A. Bekins (1998), Episodic fluid flow in the Nankai accretionary complex: Timescale, geochemistry, flow rates, and fluid budget, *J. Geophys. Res.*, *103*(B12), 351–370, doi:10.1029/98JB01983.

Saffer, D. M., and A. W. McKiernan (2005), Permeability of underthrust sediments at the Costa Rican subduction zone: Scale dependence and implications for dewatering, *Geophys. Res. Lett.*, *32*, L02302, doi:10.1029/2004GL021388.

Saffer, D. M., and E. J. Screaton (2003), Fluid flow at the toe of convergent margins: Interpretation of sharp pore-water geochemical gradients, *Earth Planet. Sci. Lett.*, *213*(3–4), 261–270.

Saffer, D. M., and H. J. Tobin (2011), Hydrogeology and mechanics of subduction zone forearcs: Fluid flow and pore pressure, *Annu. Rev. Earth Planet. Sci.*, *39*, 157–186.

Saffer, D. M., E. A. Silver, A. T. Fisher, H. Tobin, and K. Moran (2000), Inferred pore pressures at the Costa Rica subduction zone: Implications for dewatering processes, *Earth Planet. Sci. Lett.*, *177*, 193–207.
Saffer, D. M., M. B. Underwood and A. W. Mckiernan (2008), Evaluation of factors controlling smectite transformation and fluid production in subduction zones: Application to the Nankai Trough, *Island Arc*, *12*(2), 208–230.
Sahling, H., D. G. Masson, C. R. Ranero, V. Huhnerbach, W. Weinrebe, I. Klaucke, D. Burk, W. Brckmann, and E. Suess (2008), Fluid seepage at the continental margin offshore Costa Rica and southern Nicaragua, *Geochem. Geophys. Geosyst.*, *9*, Q05S05, doi:10.1029/2008GC001978.
Saito, S., and D. Goldberg (2001), Compaction and dewatering processes of the oceanic sediments in the Costa Rica and Barbados subduction zones: Estimates from in situ physical property measurements, *Earth Planet. Sci. Lett.*, *191*(3), 283–293.
Scholz, C. H. (1998), Earthquakes and friction laws, *Nature*, *391*, 37–42.
Screaton, E. J., and D. M. Saffer (2005), Fluid expulsion and overpressure development during initial subduction at the Costa Rica convergent margin, *Earth Planet. Sci. Lett.*, *233*(3), 361–374.
Screaton, E. J., D. R. Wuthrich, and S. J. Dreiss (1990), Permeabilities, fluid pressures and flow rates in the Barbados Ridge Complex, *J. Geophys. Res.*, *95*(B6), 8997–9007.
Shelley, D. R., G. C. Beroza, S. Ide, and S. Nakamula (2006), Low-frequency earthquakes in Shikoku, Japan, and their relationship to episodic tremor and slip, *Nature*, *442*(7099), 188–191.
Shi, Y., and C.-Y. Wang (1988), Generation of high pore pressures in accretionary prisms: Inferences from the Barbados subduction complex, *J. Geophys. Res.*, *93*(B8), 8893–8909.
Shipboard Scientific Party (1997a), Site 1039, *Proc. Ocean Drill. Program Initial Rep.*, *170*, 45–93.
Shipboard Scientific Party (1997b), Site 1040, *Proc. Ocean Drill. Program Initial Rep.*, *170*, 95–152.
Shipboard Scientific Party (1997e), Site 1043, *Proc. Ocean Drill. Program Initial Rep.*, *170*, 215–247.
Shipboard Scientific Party (2003), Site 1254, in *Proceedings of Ocean Drilling Program Initial Reports*, edited by J. D. Morris, H. W. Villinger, and A. Klaus, p. 205, Ocean Drill. Program, College Station, Tex.
Shipley, T. H., P. L. Stoffa, and D. F. Dean (1990), Underthrust sediments, fluid migration paths, and mud volcanoes associated with the accretionary wedge off Costa Rica: Middle America Trench, *J. Geophys. Res.*, *95*(B6), 8743–8752.
Shipley, T. H., K. D. McIntosh, E. A. Silver, and P. L. Stoffa (1992), Three-dimensional imaging of the Costa Rica accretionary prism: Structural diversity in a small volume of the lower slope, *J. Geophys. Res.*, *97*(B4), 4439–4459.
Silver, E., M. Kastner, A. Fisher, J. Morris, K. McIntosh, and D. Saffer (2000), Fluid flow paths in the Middle America Trench and Costa Rica margin, *Geology*, *28*, 679–682.
Solomon, E. A., M. Kastner, C. G. Wheat, H. Jannasch, G. Robertson, E. Davis, and J. D. Morris (2009), Long-term hydrogeochemical records in the oceanic basement and forearc prism at the Costa Rica subduction zone, *Earth Planet. Sci. Lett.*, *282*, 240–251.
Spinelli, G., and D. M. Saffer (2004), Along-strike variations in underthrust sediment dewatering on the Nicoya margin, Costa Rica, related to the updip limit of seismicity, *Geophys. Res. Lett.*, *31*, L04613, doi:10.1029/2003GL018863.
Spinelli, G., D. M. Saffer and M. Underwood (2006), Hydrogeologic responses to three-dimensional temperature variability, Costa Rica subduction margin, *J. Geophys. Res.*, *111*, B04403, doi:10.1029/2004JB003436.
Spinelli, G. A., and M. B. Underwood (2004), Character of sediment entering the Costa Rica subduction zone: Implications for partitioning of water along the plate interface, *Island Arc*, *13*(3), 432–451.
Staudigel, H., S. R Hart, and S. H. Richardson (1981), Alteration of the oceanic crust: Processes and timing, *Earth Planet. Sci. Lett.*, *52*, 311–327.
Stein, C. A., and S. Stein (1994), Constraints on hydrothermal heat flux through the oceanic lithosphere from global heat flow, *J. Geophys. Res.*, *99*(B2), 3081–3095.
Teichert, B. M. A, G. Bohrmann, and E. Suess (2005), Chemoherms on Hydrate Ridge—Unique microbially-mediated carbonate build-ups growing into the water column, *Palaeogeogr. Palaeoclimatol. Palaeoecol.*, *227*, 67–85.
Torres, M. E., B. M. A. Teichert, A. M. Trehu, W. Borowski, and H. Tomaru (2004), Relationship of pore water freshening to accretionary processes in the Cascadia margin: Fluid sources and gas hydrate abundance, *Geophys. Res. Lett.*, *31*, L22305, doi:10.1029/2004GL021219.
Underwood, M. B. (2002), Strike parallel variations in clay minerals and fault vergence in the Cascadia subduction zone, *Geology*, *30*(2), 155–158.
Underwood, M. B. (2007), Sediment inputs to subduction zones: Why lithostratigraphy and clay mineralogy matter, in *The Seismogenic Zone of Subduction Thrust Faults*, edited by T. H. Dixon and J. C. Moore, pp. 42–85, Columbia Univ. Press, N. Y.
Vannucci, P., D. W. Scholl, and M. Meschede (2001), Tectonic erosion and consequent collapse of the Pacific margin of Costa Rica: Combined implications from ODP Leg 170, seismic offshore data, and regional geology of the Nicoya Peninsula, *Tectonics*, *20*(5), 649–668.
Vannucchi, P., K. Ujiie, N. Stroncik, and V. Yatheesh (2013), IODP expedition 334: An investigation of the sedimentary record, fluid flow and state of stress on top of the seismogenic zone of an erosive subduction margin.
Voss, C. I. (1984), A finite element simulation model for saturated-unsaturated, fluid density-dependent groundwater flow with energy transport or chemically reactive single-species solute transport, *Water Resour. Invest. Rep.*, *84–4369*, U.S. Geol. Surv., Reston, Va.
Yamaguchi, A., S. F. Cox, G. Kimura, and S. Okamoto (2011), Dynamic changes in fluid redox state associated with episodic fault rupture along a megasplay fault in a subduction zone, *Earth Planet. Sci. Lett.*, *302*(3), 369–377.